Density-Functional Theory of Quantum Freezing: Sensitivity to Liquid-State Structure and Statistics

A R Denton†*, P Nielaba‡ and N W Ashcroft§

† Institut für Theoretische Physik, Technische Universität Wien, Wiedner Hauptstraße 8-10, A-1040 Wien, Austria

‡ Institut für Physik, Johannes Gutenberg Universität, Staudinger Weg 7, D-55099 Mainz, Germany

§ Laboratory of Atomic and Solid State Physics and Materials Science Center, Cornell University, Ithaca, NY 14853-2501, USA

Abstract. Density-functional theory is applied to compute the ground-state energies of quantum hard-sphere solids. The modified weighted-density approximation is used to map both the Bose and the Fermi solid onto a corresponding uniform Bose liquid, assuming negligible exchange for the Fermi solid. The required liquid-state input data are obtained from a paired phonon analysis, combined with an enhanced hypernetted-chain integral equation, and the Feynman approximation, connecting the static structure factor and the linear response function. The Fermi liquid is treated by the Wu-Feenberg cluster expansion, which approximately accounts for the effects of antisymmetry. Liquid-solid transitions for both systems are obtained with no adjustment of input data, the Fermi liquid freezing at lower density than the Bose liquid because of the destabilizing influence of fermionic statistics. Predictions for these quantum systems are shown to be more sensitive to the accuracy of the input data than is the case for the classical counterpart. Limited quantitative agreement with simulation indicates a need for still further improvement of the liquid-state input, likely through practical alternatives to the Feynman approximation.

Date: 7 February 2008

PACS number(s): 64.70.Dv, 05.70.-a, 64.60.-i, 67.80.-s

* Present address: Institut für Festkörperforschung, Forschungszentrum Jülich GmbH, D-52425 Jülich, Germany (a.denton@kfa-juelich.de)

1. Introduction

Modern density-functional (DF) theory of non-uniform systems [1] continues to yield useful insight into the fundamental nature of the liquid-solid (freezing) transition, as well as practical approximations for basic thermodynamic properties of the solid phase. Treating the solid as a highly non-uniform system, and taking as input known structural and thermodynamic properties of the corresponding uniform system, the DF approach provides an approximation for the free energy of a solid of prescribed symmetry, as a functional of the one-particle density. From the solid free energy follow freezing parameters, such as the densities of coexisting liquid and solid phases and the Lindemann ratio, as well as various solid-state properties, including the equation of state and relative stabilities of competing structures.

The Ramakrishnan-Yussouff (RY) [2] perturbative DF theory of freezing, which is based on a truncated functional Taylor-series expansion of the non-uniform system grand potential about that of the uniform liquid, initiated a number of subsequent reformulations. Among these are several non-perturbative theories, which posit a thermodynamic or structural "mapping" of the non-uniform system onto the uniform liquid. Although differing to varying extents in both philosophy and manner of approximation, all formulations of the theory require the same essential input, namely the direct correlation function (DCF) of the uniform liquid. For classical systems, the latter is trivially related to the static structure factor, which is directly obtainable from integral equation theories, simulations, or scattering experiments [3]. Numerous applications of DF theory to a wide range of bulk and interfacial systems have clearly demonstrated its utility as a practical tool for studying classical non-uniform system phenomena [4].

In recent years, extensions of the DF approach to quantum systems at zero temperature have also been developed and applied to freezing of various ground-state systems [5], including ^{4}He [6, 7], electrons [8, 9, 10] (Wigner crystallization of the Fermi one-component plasma), and Bose hard spheres [11]. For finite temperatures, a path-integral-based extension of the (classical) RY theory [12, 13] has been proposed and applied to freezing of helium. However, a general theory capable of describing freezing both in the ground state *and* at finite temperatures is still not at hand.

Ground-state quantum DF theory is formally similar to the classical theory, but a major difference is that it requires as input the quantum analog of the DCF of the uniform system. A significant complication for the quantum theory is the lack of any simple relationship between the *quantum* DCF [defined below by (8) and (9)] and the static structure factor. Since the latter is generally much easier to compute, in practice it is usually necessary to resort to approximate relationships. Unfortunately, this has tended to blur the distinction between the issues of the accuracy of the theory and the accuracy of the input to the theory. Recently, powerful quantum Monte Carlo (MC) methods have been employed to directly compute quantum DCFs for certain systems [14, 15], thereby raising the hope that more definitive tests of DF theory will

soon be possible. Nevertheless, it remains worthwhile to investigate the utility of quantum DF theory using as input the currently more accessible, if somewhat less accurate, liquid-state structural data.

In previous work [11], we extended one version of DF theory, based on the modified weighted-density approximation (MWDA) [16], from classical to ground-state quantum systems and demonstrated its application to freezing of the Bose hard-sphere (HS) liquid at zero temperature. For the liquid-state input data, we used an iterative procedure based on (*i*) the paired phonon analysis (PPA) [17] to solve the Euler-Lagrange equation for the optimum pair pseudopotential, (*ii*) the hypernetted-chain (HNC) integral equation [3] to compute the corresponding ground-state energy and static structure factor, and (*iii*) the Feynman approximation to connect the static structure factor to the quantum DCF. In an attempt to compensate for inaccuracies in the input data, we simply scaled the DCF by a constant factor at all wave vectors. Despite a favourable comparison of predicted solid ground-state energies and freezing parameters with available simulation data, the sensitivity of the results to the scaling *ansatz* remained unclear.

The main purpose of this paper is to make use of significantly more accurate data for the energy and structure of the Bose HS liquid to specifically examine the sensitivity of quantum DF theory to the quality of the liquid-state input data. In the process, we also examine the qualitative influence of particle statistics by considering freezing of both Bose and Fermi HS liquids. Aside from being of fundamental interest as idealized model systems in which effects of excluded volume interactions may be studied in isolation, HS systems also serve as useful reference systems for perturbation-theory descriptions of real quantum systems, such as helium and dense neutron matter. In Sec. 2 we begin by reviewing the principles of DF theory and the MWDA in the context of ground-state quantum systems. Section 3 concerns the structure of the liquid and describes (*i*) calculation of the static structure factor for Bose hard spheres via the PPA and an enhanced HNC integral equation that includes four- and five-body elementary diagrams [18], (*ii*) approximate connections between the static structure factor and the quantum DCF, and (*iii*) adjustment of the Bose liquid energy for Fermi statistics using the cluster expansion method of Wu and Feenberg [19]. In contrast to our previous study, *no scaling or any other modification of input data is now employed*. In Sec. 4 we outline our application of DF theory to freezing of quantum liquids and present results for hard spheres. Considerable improvement in the ground-state solid energies results from use of the more accurate liquid-state data, and distinct freezing transitions are obtained for both Bose and Fermi systems. Quantum statistics are found to significantly influence the freezing parameters, the energetically less stable Fermi liquid crystallizing at lower density, and with weaker atomic localization, than the Bose liquid. Quantitative discrepancies between theory and simulation are discussed in the context of the sensitivity of the theory to the accuracy of the input data. In Sec. 5 we summarize and conclude by suggesting the need for further improvement on the side of liquid-state theory. Finally, in

the Appendix we examine the exact short-wavelength asymptotic behaviour of the quantum DCF and possibly important implications for the accuracy of the Feynman approximation.

2. Density-Functional Theory

At zero temperature the central quantity of interest in DF theory is the total ground-state energy $E[\rho]$, a unique functional of the (spatially-varying) density $\rho(\boldsymbol{r})$ that is minimized by the equilibrium density [20], i.e.,

$$\frac{\delta E[\rho]}{\delta \rho(\boldsymbol{r})} = 0. \tag{1}$$

In general, $E[\rho]$ may be separated, according to

$$E[\rho] = E_{id}[\rho] + E_c[\rho] + E_{ext}[\rho], \tag{2}$$

into an ideal-gas energy $E_{id}[\rho]$ (energy of the non-uniform system in the absence of interactions), a correlation energy $E_c[\rho]$ due to internal interactions and exchange, and an external energy

$$E_{ext}[\rho] = \int d\boldsymbol{r}\rho(\boldsymbol{r})\phi_{ext}(\boldsymbol{r}) \tag{3}$$

due to interaction with an external potential $\phi_{ext}(\boldsymbol{r})$. One advantage of this separation is that for bosons $E_{id}[\rho]$ is given by the exact expression [11]

$$E_{id}[\rho] = \frac{\hbar^2}{2m}\int d\boldsymbol{r}|\boldsymbol{\nabla}\sqrt{\rho(\boldsymbol{r})}|^2, \tag{4}$$

where m is the particle mass. Another advantage is that $E_c[\rho]$, although not known exactly for non-uniform systems, is amenable to approximation by any of the standard DF approximations applied to the classical excess free energy. Here, as in previous work [11], we approximate $E_c[\rho]$ by an extension to ground-state quantum systems of the modified weighted-density approximation [16].

The MWDA is based on the general assumption that the non-uniform system may be mapped onto a suitably chosen uniform system [21]. In the context of ground-state quantum systems, this implies that the average correlation energy per particle of the non-uniform system is equated to that of a uniform liquid ϵ, but evaluated at an effective density $\hat{\rho}$, i.e.,

$$E_c^{MWDA}[\rho]/N \equiv \epsilon(\hat{\rho}), \tag{5}$$

where N is the number of particles. For classical solids, as well as quantum solids obeying Bose statistics, the natural choice of uniform system for the mapping is the corresponding liquid. In the case of Fermi systems, however, the effect of particle

statistics is known to be quite different in the liquid and solid phases. In particular, the exchange contribution to the energy is considerably larger in the uniform liquid than it is in the solid, in which exchanges amongst site-localized atoms are relatively rare. Comparisons of MC results for solid ^{3}He and ^{4}He [22, 23], for example, show a negligible effect of statistics on ground-state energies. Furthermore, the energies for solid ^{3}He as calculated by Ceperley *et al* [23], using a MC method to sample the square of a properly antisymmetrized wave function, are in good agreement with the VMC results of Hansen and Levesque [22], who used an unsymmetrized Jastrow trial wavefunction (see Sec. 3). These considerations motivate our assumption that within the MWDA the Fermi solid, like its Bose counterpart, is best mapped onto the corresponding Bose liquid. This is equivalent to ignoring the symmetry with respect to particle exchange of the solid many-body wavefunction, on the grounds that atoms in the solid are sufficiently localized about identifiable lattice sites as to be essentially distinguishable. The physical interpretation of the MWDA for quantum solids is thus the following: The correlation part of the ground-state energy of both the Bose *and* Fermi solids is represented by that of the corresponding Bose liquid of appropriate effective density. As this effective density is significantly lower in practice than the average solid density (see Sec. 4), the solid correlation energy is in fact modelled by that of a relatively low-density liquid, thus properly reflecting the fact that interatomic correlations are reduced upon confinement of the atoms to equilibrium lattice sites. Clearly in the case of more weakly inhomogeneous quantum systems, such as thin films or liquids near interfaces, neglect of exchange effects would be inadequate. An interesting open issue for future consideration is then how quantum DF theory might be generalized to describe Fermi systems of *arbitrary* inhomogeneity.

The effective or *weighted* density $\hat{\rho}$ is now assumed to depend on a weighted average over the volume of the system of the physical density, and is defined by

$$\hat{\rho}\equiv\frac{1}{N}\int d\boldsymbol{r}\rho(\boldsymbol{r})\int d\boldsymbol{r}'\rho(\boldsymbol{r}')w(\boldsymbol{r}-\boldsymbol{r}';\hat{\rho}), \tag{6}$$

with $\hat{\rho}$ appearing also implicitly as the argument of the weight function w. Normalization of w, according to

$$\int d\boldsymbol{r}'w(\boldsymbol{r}-\boldsymbol{r}';\rho)=1, \tag{7}$$

ensures that the approximation is exact in the limit of a uniform liquid [$\rho(\boldsymbol{r})\rightarrow\rho$]. Unique specification of w follows from further requiring that $E_c^{MWDA}[\rho]$ generate the exact "particle-hole interaction" [18] in the uniform limit, i.e.,

$$\lim_{\rho(\boldsymbol{r})\rightarrow\rho}\Big(\frac{\delta^2E_c^{MWDA}[\rho]}{\delta\rho(\boldsymbol{r})\delta\rho(\boldsymbol{r}')}\Big)=v(|\boldsymbol{r}-\boldsymbol{r}'|;\rho), \tag{8}$$

where $v(|\boldsymbol{r}-\boldsymbol{r}'|;\rho)$ is to be interpreted as the quantum analog of the classical Ornstein-Zernike two-particle DCF, henceforth referred to as the *quantum* DCF. Formally, equation (8) ensures that a functional Taylor-series expansion of $E_c^{MWDA}[\rho]$ about

the density of a uniform reference liquid is exact to second order, and also includes approximate terms to all higher orders [16, 21].

A relationship that proves useful in approximating the quantum DCF (see Sec. 3) is obtained by taking two functional derivatives of (2) and using (1), (3), and (4), yielding

$$v(|\boldsymbol{r}-\boldsymbol{r}'|;\rho) = -\frac{\delta\phi_{ext}(\boldsymbol{r})}{\delta\rho(\boldsymbol{r}')} - \frac{\delta^2 E_{id}[\rho]}{\delta\rho(\boldsymbol{r})\delta\rho(\boldsymbol{r}')} = -\Big[\chi^{-1}(|\boldsymbol{r}-\boldsymbol{r}'|;\rho) - \chi_o^{-1}(|\boldsymbol{r}-\boldsymbol{r}'|;\rho)\Big], \quad (9)$$

where

$$\chi^{-1}(|\boldsymbol{r}-\boldsymbol{r}'|;\rho) = \frac{\delta\phi_{ext}(\boldsymbol{r})}{\delta\rho(\boldsymbol{r}')} \quad (10)$$

is the functional inverse of the static density-density linear response function and

$$\chi_o^{-1}(|\boldsymbol{r}-\boldsymbol{r}'|;\rho) = -\frac{\delta^2 E_{id}[\rho]}{\delta\rho(\boldsymbol{r})\delta\rho(\boldsymbol{r}')}. \quad (11)$$

is its non-interacting (free-particle) limit. The Fourier transform of the latter can be expressed [using (4)] in the simple form

$$\chi_o^{-1}(k) = -\frac{\hbar^2 k^2}{4m\rho}. \quad (12)$$

In Fourier space, where computations are most conveniently carried out, the weight function is given by the analyic relation

$$w(k;\rho) = \frac{1}{2\epsilon'(\rho)}\Big[v(k;\rho) - \delta_{k,0}\rho\epsilon''(\rho)\Big], \quad (13)$$

which follows directly from (5)-(8). Note that normalization of the weight function implies, via (13), the quantum compressibility sum rule

$$v(k=0;\rho) = 2\epsilon'(\rho) + \rho\epsilon''(\rho) = mc^2/\rho, \quad (14)$$

c being the speed of longitudinal sound. This sets a consistency constraint on the liquid-state energy and structure.

In summary, equations (5), (6), (7), and (13) constitute the MWDA for the correlation energy of a quantum solid at zero temperature. Practical implementation of the theory requires knowledge of the liquid-state correlation energy ϵ and the quantum DCF v, the subject of the next section.

3. Liquid-State Energy and Structure

For the ground-state Bose HS system, the liquid-state energy and static structure factor have been obtained by a method that combines the paired phonon analysis (PPA) [17] with integral equation theory. The extraction of the key quantum DCF

from the static structure factor is described in detail below. First, however, we briefly summarize the PPA.

The basis of the PPA, as well as of variational Monte Carlo (VMC) methods, is a trial ground-state wavefunction of the general Feenberg form

$$\psi_B(\boldsymbol{r}_1,\ldots,\boldsymbol{r}_N) = \exp[-\sum_{i<j} u_2(\boldsymbol{r}_i,\boldsymbol{r}_j) - \sum_{i<j<k} u_3(\boldsymbol{r}_i,\boldsymbol{r}_j,\boldsymbol{r}_k) - \cdots], \qquad (15)$$

from which the optimum correlation factors u_n are determined by minimization of the total ground-state energy, according to

$$\frac{\delta}{\delta u_n}\left[\frac{\langle\psi_B|H|\psi_B\rangle}{\langle\psi_B|\psi_B\rangle}\right] = 0, \qquad (16)$$

where H is the Hamiltonian. In order to be able to directly compare with results of VMC simulations, we mainly concern ourselves here with a trial wavefunction of the Jastrow form, which includes only the pair correlation factor, or pseudopotential, $u_2(r) \equiv u(r)$. We have also considered, however, the effect of including triplet correlations and briefly comment on this in Sec. 4. The pseudopotential is constrained by the general condition that $u(r)\to 0$ as $r \to \infty$, implying vanishing correlations at infinite separation, and the condition (specific to hard spheres of diameter σ) that $u(r) \to \infty$ as $r \to \sigma$, ensuring a minimum pair separation of σ. In applications to solids, VMC methods assume (15) multiplied by a product of one-body (typically Gaussian) wavefunctions, each centred on a lattice site.

By exploiting the formal correspondence between the quantum probability density $|\psi_B|^2$ and the classical Boltzmann factor [24], in which $u(r)$ may be interpreted as a classical pair potential, the method uses integral equation theory for *classical* liquids to determine the radial distribution function $g(r,[u])$ for a given $u(r)$. In previous work [11], we used the approximate HNC integral equation, which entirely neglects the bridge function. Here, we use a more accurate enhancement of the HNC equation (denoted by "HNC+") that approximates the bridge function by four- and five-body elementary diagrams. From $g(r,[u])$, the corresponding correlation energy is computed via [17, 24]

$$E_c(\rho) = \frac{1}{2}\rho \int d\boldsymbol{r} g(r,[u])[\frac{\hbar^2}{2m}\nabla^2 u(r) + \phi(r)], \qquad (17)$$

where $\phi(r)$ is the pair potential (for hard spheres in our case). The random phase approximation is then used iteratively to adjust the pseudopotential until the energy is minimized. Figure 1 illustrates the resulting static structure factor $S(k)$, which is related to $g(r)$ by the Fourier transform relation

$$S(k) = 1 + \rho \int d\boldsymbol{r}[g(r) - 1]\exp(i\boldsymbol{k}\cdot\boldsymbol{r}). \qquad (18)$$

To date there is no known exact relation connecting $S(k)$ to the quantum DCF $v(k)$. However, as shown in Sec. 2, $v(k)$ is trivially related to the static response

function $\chi(k)$. Further, the fact that $S(k)$ and $\chi(k)$ may be expressed as frequency moments

$$m_p(k) = \int_0^\infty d\omega (\hbar\omega)^p S(k,\omega), \tag{19}$$

of the dynamic structure factor $S(k,\omega)$ provides a basis for approximations [25]. The relevant lowest-order moments (or sum rules) are given explicitly by

$$m_{-1} = -\frac{1}{2\rho}\chi(k), \tag{20}$$

$$m_0 = S(k), \tag{21}$$

and

$$m_1 = \frac{\hbar^2 k^2}{2m}. \tag{22}$$

From the rigorous inequality

$$\int_0^\infty d\omega \frac{S(k,\omega)}{\hbar\omega}(1 + a\hbar\omega)^2 = m_{-1} + 2am_0 + a^2 m_1 \geq 0, \tag{23}$$

variation of the real parameter a to minimize the left-hand side yields the bound [25]

$$m_{-1}(k) \geq \frac{2mS^2(k)}{\hbar^2 k^2}. \tag{24}$$

The treatment of (24) as an equality, rather than merely as an upper bound, is the so-called Feynman approximation,

$$m_{-1}^F(k) = \frac{2mS^2(k)}{\hbar^2 k^2}. \tag{25}$$

From (9), (12), and (20), the corresponding Feynman approximation for $v(k)$ is

$$v^F(k) = \frac{\hbar^2 k^2}{4m\rho}\Big(\frac{1}{S^2(k)} - 1\Big), \tag{26}$$

which is plotted in Figure 2 for Bose hard spheres, using the PPA $S(k)$.

In the long-wavelength ($k \to 0$) limit, the Feynman approximation evidently correctly obeys (14), since $S(k)$ is known to vanish linearly with k, according to [26]

$$S(k) \sim \frac{\hbar k}{2mc} \quad (k \to 0). \tag{27}$$

However, the PPA – in common with all liquid theories – does not satisfy the compressibility sum rule [equation (14)] relating ϵ and $v(k=0)$. That is, the speed of longitudinal sound derived from ϵ differs from that derived from $v(k=0)$. At $k=0$ the discrepancy is unimportant, since the MWDA satisfies the sum rule by construction

[see (7) and (13)]. At $k \neq 0$ any remnant of the discrepancy is important only to the extent that $v(k)$ may be affected at relevant wave vectors, e.g., the reciprocal lattice vectors of the crystal in the application to freezing (Sec. 4). Recently a simple analytic modification of $v(k)$ has been introduced [27] to correct the low-k behaviour. This correction, however, would have negligible effect on $v(k)$ at the wave vectors relevant to freezing, since the first reciprocal lattice vector of the crystal generally lies at or beyond the first minimum in $v(k)$ (see Figure 2). Thus, although in previous work [11] the sum rule violation motivated an empirical scaling of $v(k)$, in the present work we make *no alteration to the PPA input*.

In the opposite short-wavelength ($k \to \infty$) asymptotic limit, it may be shown from (26) that $v^F(k) \to 0$, which is identical to the corresponding limit of the classical DCF. In the Appendix we consider a recently-proposed extension to the Feynman approximation, involving higher-order moments of $S(k,\omega)$, and use this to analyse the *exact* asymptotic behaviour of $v(k)$. Interestingly, unlike its classical counterpart, the exact quantum DCF tends not to zero, but rather to a density-dependent constant. The same property has been discussed recently, in another context, by Likos et al [28], and may have important implications for the form of the exact quantum DCF in the finite-k range of relevance for the DF theory of quantum solids.

For the Fermi HS liquid, we have approximated the ground-state energy by adjusting the Bose liquid energy for Fermi statistics using the Wu-Feenberg (or Pandharipande-Bethe) cluster expansion method [19]. The same approach has been adopted previously in VMC studies of liquid ^{3}He [22] and of the Fermi HS liquid [29]. The Wu-Feenberg (WF) method assumes that the Pauli exclusion principle acts only as a weak perturbative correction to the strongly repulsive pair potential, and it takes as a trial wavefunction ψ_F the Bose wavefunction ψ_B antisymmetrized by a Slater determinant:

$$\psi_F(\boldsymbol{r}_1,\ldots,\boldsymbol{r}_N) = \psi_B(\boldsymbol{r}_1,\ldots,\boldsymbol{r}_N)\cdot\det[\exp(i\boldsymbol{k}_i\cdot\boldsymbol{r}_j)]. \tag{28}$$

The corresponding ground-state energy per particle ϵ^F may be expressed as a cluster expansion about the Bose counterpart ϵ^B, according to

$$\epsilon^F = \epsilon^B + \epsilon_0^F + \epsilon_1^F + \epsilon_2^F, \tag{29}$$

where

$$\epsilon_0^F = \frac{3}{5}\epsilon_F, \tag{30}$$

$$\epsilon_1^F = 24\epsilon_F \int_0^1 dx x^4 (1 - \frac{3}{2}x + \frac{1}{2}x^3)[S(2k_F x) - 1], \tag{31}$$

and

$$\epsilon_2^F = -\Big(\frac{3}{8\pi}\Big)^3 \epsilon_F \int d\boldsymbol{x}_1 \int d\boldsymbol{x}_2 \int d\boldsymbol{x}_3 x_{12}^2 S(k_F x_{12})[S(k_F x_{23}) - 1][S(k_F x_{31}) - 1], \tag{32}$$

with $k_F = (3\pi^2\rho)^{1/3}$ and $\epsilon_F = (\hbar^2 k_F^2/2m)$ being the Fermi wave-vector and energy, respectively, and with the integrals in (32) extending over the unit sphere. Evidently ϵ_0^F is the one-particle correction arising directly from the Pauli exclusion principle for non-interacting fermions, while ϵ_1^F and ϵ_2^F arise from antisymmetrization of two- and three-particle clusters, respectively. We have computed the first-order correction ϵ_1^F by standard numerical quadrature and the second-order correction ϵ_2^F by a simple Monte Carlo integration algorithm that randomly chooses triplets of points within the nine-dimensional integration volume. Figure 3 shows the resulting relative magnitudes of successive terms in the cluster expansion.

At first glance, the apparent rapid convergence of the first few terms in the WF expansion would seem to lend some *a posteriori* justification to the assumption of a small perturbation. Serious doubts have been raised, however, concerning the general convergence properties of such cluster expansions [23, 30, 31]. Brandow [30] has identified two distinct antisymmetry effects and argued that one of these, the so-called "correlation-exclusion" effect, is treated in a non-converging manner, and in fact can be properly accounted for only by including diagrams involving exchanges amongst any number of particles up to and including all N particles. The MC calculations of Ceperley *et al*, for a variety of pair-wise-interacting Fermi systems, demonstrate that the WF expansion tends to consistently underestimate the energy, particularly for soft-core pair potentials and at high densities. Krotscheck [32] has shown that conventional cluster expansion methods tend to be unreliable in the case of high densities and long-ranged Jastrow functions, and stressed the importance of summing to all orders certain properly combined classes of diagrams (Fermi chains). The Fermi HNC method, although summing much larger classes of diagrams than the WF expansion, also is plagued by uncertain convergency [32]. Despite the somewhat doubtful convergence properties of the WF expansion, we nevertheless employ it here, pending a more accurate treatment of the Fermi liquid [33], in order to make contact with the available VMC simulation data [29], and to estimate – at least qualitatively – the influence of Fermi statistics on the freezing parameters of hard spheres.

4. Freezing of Quantum Hard Spheres

The main steps in applying DF theory to bulk solids and freezing transitions are parametrization of the solid density, minimization of the total solid energy with respect to the parametrized density, and identification of liquid-solid coexistence by construction of a Maxwell common tangent. Below we outline the procedure, which is described in greater detail elsewhere [11].

Assuming a Gaussian density distribution about the lattice sites of a perfect *fcc* crystal, the solid density takes the form

$$\rho_s(\boldsymbol{r}) = (\frac{\alpha}{\pi})^{\frac{3}{2}} \sum_{\boldsymbol{R}} \exp(-\alpha|\boldsymbol{r} - \boldsymbol{R}|^2), \tag{33}$$

where the localization parameter α determines the width of the Gaussians centred on the lattice sites at positions $\boldsymbol{R}$. This choice corresponds to including a Gaussian one-body factor in the trial wavefunction of (15). We focus here on the *fcc* crystal structure, since solid helium is known from experiment to assume a close-packed structure at zero temperature and corresponding pressures [34], and since our previous study indicated negligible differences between the relative stabilities of *fcc*, *hcp*, and *bcc* structures. The Gaussian *ansatz* has been widely adopted in applications of DF theory to *classical* systems [1, 4]. Simulation studies by Young and Alder [35] and by Ohnesorge *et al* [36] have demonstrated the global form of the classical HS crystal density distribution to be close to Gaussian, especially near close packing, although near melting the tails of the distribution do exhibit significant anisotropic deviations of roughly 10% from the Gaussian form [36]. The only comparable study for quantum systems that we are aware of is the Green's Function Monte Carlo (GFMC) simulation of Whitlock *et al* [37] for a Lennard-Jones model of ^{4}He, which found a spherically symmetric density distribution about a given lattice site with only small positive deviations from Gaussian behaviour in the tail of the distribution. Since freezing properties are known to be dominated by short-range repulsive forces, which are similar in HS and Lennard-Jones systems, we can expect the Gaussian *ansatz* also to be a reasonable approximation for quantum hard spheres. Caution is warranted, however, in this application to a relatively low-density quantum solid to the extent that the solid energy may be sensitive to anisotropy and other deviations of the density from the simple Gaussian form. A definitive resolution of the issue could be obtained by the technique of free minimization [36], which avoids entirely the need for density parametrization, although we have not attempted such an extensive computation.

From (13) and (33), (6) now takes the form

$$\hat{\rho}(\alpha, \rho_s) = \rho_s \Big[1 + \frac{1}{2\epsilon'(\hat{\rho})} \sum_{\boldsymbol{G} \neq 0} \exp(-G^2/2\alpha) v(G; \hat{\rho}) \Big], \tag{34}$$

where ρ_s is the average solid density and G the magnitude of the *fcc* reciprocal lattice vector $\boldsymbol{G}$. Given the liquid-state functions $\epsilon(\rho)$ and $v(k; \rho)$ from Sec. 3, this implicit relation for $\hat{\rho}$ can be easily solved by numerical iteration at fixed α and ρ_s. From $\hat{\rho}$ the approximate correlation energy E_c^{MWDA} then follows immediately from (5).

It is important to emphasize that here we map both the Bose and the Fermi HS solids onto the corresponding Bose liquid, under the assumption that exchange effects in the Fermi solid are negligible. As noted in Sec. 2, this assumption is expected to be valid in the solid, where overlap of neighbouring density distributions is negligible. In this case, the ideal-gas energy E_{id} takes the simple analytic form [11]

$$E_{id}/N \simeq \frac{3}{4} \frac{\hbar^2}{m} \alpha, \tag{35}$$

identical to the form usually assumed in VMC simulations [22]. Assuming no external potential, (5) and (35) combine finally to give the approximate total energy per particle

$$E^{MWDA}(\alpha, \rho_s)/N \simeq \frac{3}{4} \frac{\hbar^2}{m} \alpha + \epsilon(\hat{\rho}(\alpha, \rho_s)). \tag{36}$$

Note that in the case of helium the mass difference between the ^{3}He and ^{4}He isotopes gives rise to quite different kinetic contributions to the total energy. For the purely kinetic HS systems considered here, however, the energies of the Bose and Fermi solids (in units of $\hbar^2/2m\sigma^2$) are identical by assumption.

Minimization of (36) with respect to the single variational parameter α (at fixed ρ_s) is illustrated in Figure 4, which shows separately the variation of the ideal-gas and correlation energies with α. The linear increase of E_{id}, which results from the kinetic energy cost of increasing the curvature of the one-particle wavefunction, strongly opposes localization of the atoms about their lattice sites. In contrast, the rapid decrease of E_c, which arises from a weakening of interactions with reduced overlap of neighbouring density distributions, strongly favours localization. At sufficiently high density, the competition between E_{id} and E_c results in a minimum in the *total* energy at non-zero α, signalling mechanical stabilization of the solid. By varying ρ_s and repeating the above minimization procedure, the solid equation of state (E vs ρ_s) is obtained. Figure 5 displays the corresponding weighted density, confirming the characteristic trait of the MWDA, referred to in Sec. 2, that $\hat{\rho}$ is always lower than the average solid density. It should be noted that Figure 5 differs from the corresponding figure in [11] (second reference) due to a plotting error in the latter, and that the roughness of the curve arises from linear interpolation between grid points of the liquid-state $v(k)$.

Thermodynamic stability of the solid is assessed by comparing the liquid and solid energies. Coexistence between liquid and solid, characterized by equality of the pressures and of the chemical potentials in the two phases, may be established by constructing a common tangent – *if one exists* – to the energy vs. density curves, the coexistence densities occurring at the points of common tangency. The corresponding value of α determines the Lindemann ratio L, defined as the ratio of the *rms* atomic displacement to the nearest-neighbour distance in the solid at coexistence. For the *fcc* crystal $L = (3/\alpha a^2)^{1/2}$, where a is the lattice constant.

Applying the above procedure, we have computed the energy as a function of density for the ground-state quantum HS *fcc* crystal and have attempted a freezing analysis for the Bose and Fermi systems. In order to assess the sensitivity of the theory to the accuracy of the liquid-state input data, we have performed calculations for the Bose system using data generated by the PPA with both the simple HNC and the enhanced HNC+ approximations restricted to pair correlations (see Sec. 3). The PPA static structure factor – and hence the quantum DCF [from (26)] – turns out to be practically identical regardless of whether the HNC or HNC+ closure is used. The energy, however, differs significantly. Figure 6 shows the Bose HS liquid energy density vs number density in the two approximations, together with the corresponding *fcc* crystal energy density predicted by our DF theory. Also shown, for comparison, are the VMC simulation data of Hansen *et al* [22]. In both cases, the existence of a common tangent to the liquid and solid curves confirms the occurrence of a freezing transition. The corresponding freezing parameters are given in Table 1, where it

is seen that in comparison with simulation the theory considerably overestimates the coexistence densities as well as the density change, and underestimates the Lindemann ratio. Evidently, use of the more accurate HNC+ approximation significantly improves agreement with simulation for both the liquid and solid energies. In fact, the liquid energy agrees almost perfectly up to $\rho\sigma^3 = 0.4$, well beyond the freezing density. Nevertheless, the coexistence densities are slightly more accurate within the HNC approximation, highlighting the delicate dependence of the freezing parameters on the detailed form of the equation of state. Despite quantitative discrepancies in the predicted freezing parameters, it is important to point out that the prediction of a freezing transition itself is a significant qualitative result, considering that the second-order RY version of DF theory gives no freezing transition for the same input data [6, 7].

To test for sensitivity of the results to the assumption of pair correlations in the trial wavefunction of (15), we have repeated the calculations using PPA input data that include triplet correlations. Although the liquid $S(k)$, and hence the quantum DCF, is essentially the same as with pair correlations, the liquid energies are slightly lowered. This results in a consistent lowering also of the solid energies and a slight reduction in the densities of coexisting liquid and solid, indicating that comparisons with highly accurate simulation data, not restricted to pair correlations, should properly incorporate triplet correlations. In comparison with more accurate GFMC simulation data [38], however, the predicted solid energies and freezing densities are still significantly overestimated. For clarity, it is important to distinguish between higher-order correlation factors in the trial wavefunction of the liquid-state theory and higher-order DCFs in the approximate energy functional in the DF theory of the solid. Although here only the pair DCF is explicitly invoked through (8), in principle the theory could be extended to include also higher-order DCFs, defined as higher-order functional derivatives of the energy functional, as in fact has been achieved already, at the level of the triplet DCF, in the classical theory [39].

The same procedure as above has been applied to the Fermi HS system, in this case though, using only the more accurate PPA-HNC+ input with pair correlations. Figure 7 shows the Fermi liquid and *fcc* crystal energy densities together with the Bose liquid energy and the corresponding VMC data of Schiff [29] for comparison. We reiterate here that the Fermi liquid energy is approximated by the sum of the Bose liquid energy and the WF corrections shown in Figure 3. Of course, because the VMC data also are based on the WF expansion for the liquid and on the neglect of exchange effects in the solid, the comparison, although consistent, is not a test of the validity of these two approximations. The predicted Fermi system freezing parameters are listed in Table 1, where the relative change of density upon freezing is seen to be about 4 %. Unfortunately, the scarce available simulation data [29] do not permit an accurate determination of freezing parameters for comparison. For convenience, the predicted energy densities for both Bose and Fermi systems from Figures 6 and 7 are listed numerically in Tables 2 and 3. Note that the higher energy of the Fermi liquid compared with that of the Bose liquid simply reflects the destabilizing effect of

Fermi statistics (exchange) on the liquid phase and naturally leads to a lowering of the liquid and solid coexistence densities, as is observed experimentally in the case of ^{3}He and ^{4}He [34]. Considering the sensitivity of the freezing parameters to details of the equation of state, however, quantitative predictions must await a more accurate treatment of the Fermi liquid [33].

The consistent over-prediction of solid energies points to a systematic error either in the theory or in the input to the theory. To investigate this issue, it is instructive to compare the present results with those found previously by a similar analysis [11]. In the previous study, empirical scaling of the liquid-state DCF by a factor of roughly 1.2 considerably improved the freezing parameters. Similar conclusions have been reached by other workers [6, 7] who applied the RY version of DF theory to ^{4}He. On the assumption that the MWDA is basically reliable, at least for HS systems, this observation would suggest that the true $v(k)$ is considerably more structured than that predicted by the current PPA-based liquid-state theory. Indeed, calculations and comparison with experiments for liquid ^{4}He have shown [40, 41] that the Feynman approximation tends to underestimate the structure of the static response function, especially in the crucial region near the roton maximum. This is evidence that the incorrect asymptotic behaviour of $v^F(k)$ (see Appendix) may be adversely affecting the relevant finite-k region. In quantum freezing, the k-range of practical interest is considerably narrower than in classical systems. This is because the quantum solid has a much lower density near the transition than the classical solid, and hence a much wider Gaussian density distribution. Included in Figure 2 are the positions and relative weights of the first few *fcc* reciprocal lattice vectors, illustrating that the region of the first minimum, and to a lesser extent the second minimum, of $v(k)$ is crucial in determining the weighted density and thus the energy of the solid. The fact that $S(k)$ is relatively insensitive to the type of closure approximation used (HNC or HNC+) suggests that it is the Feynman approximation [equation (26)], in converting $S(k)$ to $v(k)$, that is most likely responsible for any significant error in $v(k)$. Finally, it should be noted that any remaining high-density error in the PPA calculation of the input liquid energy will have negligible effect on the solid energy, since the MWDA always maps the solid onto an effective liquid of lower density (see Figure 5). Thus, the only option for improving the theoretical results appears to lie in the input of a more accurate liquid-state DCF, respecting the correct asymptotic limit.

5. Summary and Conclusions

By way of recapitulation, we have applied density-functional theory of non-uniform systems to quantum hard-sphere solids at zero temperature, and thereby studied the liquid-solid transition of Bose and Fermi systems. Mapping both the Bose and Fermi solids onto the corresponding Bose liquid through the use of the modified weighted-density approximation, ignoring exchange effects in the Fermi solid, and taking liquid-state input data from an accurate paired phonon analysis calculation coupled with

the Feynman approximation, the solid energy and freezing parameters have been computed with no adjustable parameters. The qualitative influence of Fermi statistics on the freezing transition also has been considered by using the Wu-Feenberg cluster expansion method to approximate the effect of antisymmetry on the Fermi liquid energy. Compared with the Bose liquid, the energetically less stable Fermi liquid freezes at lower density into a lower-density solid with a higher Lindemann ratio.

The ground-state energies obtained using liquid-state input data of varying degrees of accuracy are generally in satisfactory qualitative agreement with available simulation data. Furthermore, distinct liquid-solid transitions are always obtained, demonstrating a certain robustness of the theory. Quantitative accuracy depends heavily, however, on the accuracy of the input data. The freezing parameters, in particular, are especially sensitive to the detailed form of the equation of state. As shown previously for Bose hard spheres [11], empirical scaling of the Feynman DCF (or static response function) by an appropriate structure-enhancing factor results in much closer agreement with simulation than is obtained by using the best available unscaled liquid-state data. Experience with ^{4}He further indicates that the Feynman approximation tends to underestimate the structure of the liquid. Finally, analysis of the short-wavelength asymptotic behaviour of the exact liquid DCF reveals that the Feynman DCF tends to the wrong limit. We conclude therefore that a more accurate liquid-state DCF – generated either through alternatives to the Feynman approximation or by Quantum Monte Carlo simulation – is still called for to achieve a decisive quantitative test of the theory in this demanding application.

Acknowledgments

We are grateful to E Krotscheck for his interest in the work and for supplying the PPA data, and to C N Likos for sending a preprint of Ref. [28] prior to publication. This work was supported by the Materials Science Center at Cornell University and through NSF Grant No DMR 9319864. ARD gratefully acknowledges support at various stages from the Natural Sciences and Engineering Research Council of Canada and from the Austrian Science Foundation. PN thanks the DFG (Heisenberg Foundation) for support.

Appendix. Asymptotic Limit of $v(k)$

As discussed in Sec. 3, analysis of the lowest-order frequency moments of $S(k,\omega)$ leads directly to the Feynman approximation for $v(k)$, which is seen [from (26) and (27)] to have the asymptotic limit $v^F(k) \to 0$ as $k \to \infty$. The moment analysis may be straightforwardly extended [41] to include the higher-order moments m_2 and m_3. The latter may be expressed in the form [25, 41]

$$m_2 = \Big(\frac{\hbar^2 k^2}{2m}\Big)^2 \Big[2 - S(k)\Big] + \frac{\hbar^4 k^2}{m^2} D(k), \tag{A1}$$

where $D(k)$ is the kinetic structure function, defined by

$$D(k) \equiv \int d\boldsymbol{r} \int d\boldsymbol{r}' \cos(k(z-z'))\nabla_z \nabla_{z'} \rho^{(2)}(\boldsymbol{r}, \boldsymbol{r}'; \boldsymbol{R}, \boldsymbol{R}')|_{\{\boldsymbol{r},\boldsymbol{r}'\}=\{\boldsymbol{R},\boldsymbol{R}'\}}, \tag{A2}$$

and

$$m_3 = \Big(\frac{\hbar^2 k^2}{2m}\Big)^3 + \Big(\frac{\hbar^2 k^2}{m}\Big)^2 \langle \epsilon_K \rangle + \frac{\hbar^4 \rho}{2m^2} \int d\boldsymbol{r} g(r)[1 - \cos(\boldsymbol{k}\cdot\boldsymbol{r})](\boldsymbol{k}\cdot\nabla)^2 \phi(r), \tag{A3}$$

with $\langle \epsilon_K \rangle$ the mean ground-state kinetic energy per particle and $\phi(r)$ the interatomic potential. Starting from the rigorous inequality

$$\int_0^\infty d\omega \frac{S(k,\omega)}{\hbar\omega}(1 + a\hbar\omega + b\hbar^2\omega^2)^2 \geq 0, \tag{A4}$$

and minimizing the left-hand side with respect to the real parameters a and b, yields the bound

$$m_{-1}(k) \geq \frac{m_{-1}^F(k)}{1 - \Delta(k)/\epsilon(k)}, \tag{A5}$$

where

$$\Delta(k) = \frac{m_2}{m_1} - \frac{m_1}{m_0} \tag{A6}$$

and

$$\epsilon(k) = \Big[\frac{m_3}{m_1} + \Big(\frac{m_1}{m_0}\Big)^2 - 2\frac{m_2}{m_o}\Big]/\Delta(k). \tag{A7}$$

Treating (A5) as an equality, and using (9), (12), and (20), leads to the approximation

$$v(k) = \frac{\hbar^2 k^2}{4m\rho}\Big[\frac{1}{S^2(k)}\Big(1 - \Delta(k)/\epsilon(k)\Big) - 1\Big], \tag{A8}$$

which in principle represents an improvement over the Feynman approximation. Indeed, for ^{4}He the corresponding density-density static response has been explicitly computed by quantum MC and shown to significantly improve the comparison with experiment [14]. Since the kinetic structure function is not readily available for hard spheres, however, we have not attempted to use (A8) in this paper. Nevertheless, it is interesting to consider the asymptotic short-wavelength limit. This is straightforward, since it is known [25] that

$$D(k) \to \frac{2}{3}\frac{m}{\hbar^2}\langle \epsilon_K \rangle \quad (k \to \infty) \tag{A9}$$

and since for hard spheres $m_3(k)$ may be explicitly expressed as [42]

$$\begin{aligned} m_3 = \Big(\frac{\hbar^4 k^4}{2m^2}\Big)mc^2 + \Big(\frac{\hbar^2 k^2}{2m}\Big)^3 + \Big(\frac{\hbar^2 k^2}{m}\Big)^2 \Big[\Big(\frac{P}{\rho} - \frac{2}{3}\langle \epsilon_K \rangle\Big)\Big(\mathcal{P}_1(k\sigma) - 1\Big) \\ + \Big(mc^2 - \frac{2P}{\rho} - \frac{2}{3}\langle \epsilon_K \rangle\Big)\Big(\mathcal{P}_2(k\sigma) - \frac{1}{2}\Big)\Big], \end{aligned} \tag{A10}$$

where P is the pressure and

$$\mathcal{P}_1(x) \equiv \frac{3}{x^2}\Big(\frac{\sin x}{x} - \cos x\Big), \tag{A11}$$

$$\mathcal{P}_2(x) \equiv \frac{5}{x^2}\Big[\frac{1}{3} + \frac{2}{x^2}\Big(\frac{\sin x}{x} - \cos x\Big) - \frac{\sin x}{x}\Big]. \tag{A12}$$

The various moments appearing in (A6) and (A7) are easily shown to behave asymptotically as

$$m_0 \to 1, \tag{A13}$$

$$m_1 \to \frac{\hbar^2 k^2}{2m}, \tag{A14}$$

$$m_2 \to \Big(\frac{\hbar^2 k^2}{2m}\Big)^2 + \frac{2}{3}\frac{\hbar^2 k^2}{m}\langle \epsilon_K \rangle, \tag{A15}$$

and

$$m_3 \to \Big(\frac{\hbar^2 k^2}{2m}\Big)^3 + \Big(\frac{\hbar^2 k^2}{m}\Big)^2 \langle \epsilon_K \rangle. \tag{A16}$$

Substituting these limits into (A6) and (A7), we obtain

$$\Delta(k)/\epsilon(k) \to \frac{8}{3}\frac{m\langle \epsilon_K \rangle}{\hbar^2 k^2}, \tag{A17}$$

which, upon further substitution into (A8), yields

$$v(k) \to -\frac{2}{3}\frac{\langle \epsilon_K \rangle}{\rho}. \tag{A18}$$

Thus, the exact $v(k)$ approaches a *finite* negative constant as $k \to \infty$, in sharp contrast to the asymptotic vanishing of the Feyman approximation, as well as of the classical DCF. It is interesting to note that analogous behaviour has been derived for the corresponding function defined for the uniform electron liquid [43]. In fact, as has been recently suggested [28], it is quite probably a universal feature of quantum DCFs. What this curious asymptotic behaviour may imply for the *finite-k* behaviour of the true $v(k)$ of Bose hard spheres remains to be clarified by a decisive quantum MC computation.

References

[1] For reviews of the basic principles of DF theory see Evans R 1979 *Adv. Phys.* **28** 143; Evans R 1989, in *Liquids at Interfaces*, Les Houches session 48, edited by Charvolin J, Joanny J F and Zinn-Justin J (New York: Elsevier); Oxtoby D W, 1990 in *Liquids, Freezing and Glass Transition*, Les Houches session 51, edited by Hansen J-P, Levesque D and Zinn-Justin J (New York: Elsevier)

[2] Ramakrishnan T V and Yussouff M 1979 *Phys. Rev.* B **19** 2775; Haymet A D J and Oxtoby D W 1981 *J. Chem. Phys.* **74** 2559

[3] Hansen J-P and McDonald I R 1986 *Theory of Simple Liquids* 2^{nd} edition (London: Academic)

[4] For recent reviews of applications of DF theory see Löwen H *Phys. Reports* 1994 **237** 249; Singh Y 1991 *Phys. Reports* **207** 351

[5] For reviews of quantum DF theory see Moroni S and Senatore G 1994 *Phil. Mag.* B **69** 957; Haymet A D J 1992 in *Inhomogeneous Fluids* edited by Henderson D (New York: Dekker)

[6] Moroni S and Senatore G 1991 *Europhys. Lett.* **16** 373

[7] Dalfovo F, Dupont-Roc J, Pavloff N, Stringari S and Treiner J 1991 *Europhys. Lett.* **16** 205

[8] Senatore G and Pastore G 1990 *Phys. Rev. Lett.* **64** 303

[9] Moroni S and Senatore G 1991 *Phys. Rev.* B **44** 9864

[10] Choudhury N and Ghosh S K 1995 *Phys. Rev.* B 51 2588

[11] Denton A R, Nielaba P, Runge K J and Ashcroft N W 1990 *Phys. Rev. Lett.* **64** 1529; 1991 *J. Phys. Condens. Matter* **3** 593

[12] McCoy J D, Rick S W and Haymet A D J 1989 *J. Chem. Phys.* **90** 4622; 1990 *J. Chem. Phys.* **92** 3034

[13] Rick S W, McCoy J D and Haymet A D J 1990 *J. Chem. Phys.* **92** 3040

[14] Moroni S, Ceperley D M and Senatore G 1992 *Phys. Rev. Lett.* **69** 1837

[15] Moroni S, Ceperley D M and Senatore G 1995 *Phys. Rev. Lett.* **75** 689

[16] Denton A R and Ashcroft N W 1989 *Phys. Rev.* A **39** 4701

[17] Chang C C and Campbell C E 1977 *Phys. Rev.* B **15** 4238; Jackson H W and Feenberg E 1961 *Ann. Phys.* **15** 266

[18] Krotscheck E and Saarela M 1993 *Phys. Rep.* **232** 1; Krotscheck E 1986 *Phys. Rev.* B **33** 3158

[19] Wu F Y and Feenberg E 1962 *Phys. Rev.* **128** 943; Pandharipande V R and Bethe H A 1973 *Phys. Rev.* C **7** 1312

[20] Hohenberg P and Kohn W 1964 *Phys. Rev.* **136** B864

[21] Curtin W A and Ashcroft N W 1985 *Phys. Rev.* A **32** 2909; 1986 *Phys. Rev. Lett.* **56** 2775; 1986 **57** 1192 erratum

[22] Hansen J-P and Levesque D 1968 *Phys. Rev.* **165** 293; Hansen J-P, Levesque D and Schiff D 1971 *Phys. Rev.* A **3** 776

[23] Ceperley D, Chester, G V and Kalos M H 1977 *Phys. Rev.* B **16** 3081

[24] McMillan W L 1965 *Phys. Rev.* **138** A 442

[25] Hall D and Feenberg E 1971 *Ann. Phys.* **63** 335

[26] Chester G V and Reatto L 1966 *Phys. Lett.* **22** 276

[27] Campbell C E, Folk R and Krotscheck E 1997 *J. Low Temp. Phys.* in press

[28] Likos C N, Moroni S and Senatore G 1997 *Phys. Rev.* B in press

[29] Schiff D 1973 *Nature Phys. Sci.* **243** 130

[30] Brandow B H 1976 *Phys. Lett.* B **61** 117

[31] Krotscheck E 1976 *Lett. Nuov.* C **16** 269; Krotscheck E and Takahashi K 1976 *Phys. Lett.* B **63** 269

[32] Krotscheck E 1977 *Nucl. Phys.* A **293** 293; 1977 *J. Low Temp. Phys.* **27** 199

[33] Krotscheck E and Denton A R unpublished

[34] Wilks J 1967 *The Properties of Liquid and Solid Helium* (Clarendon: Oxford University Press)

[35] Young D A and Alder B J 1974 *J. Chem. Phys.* **60** 1254

[36] Ohnesorge R, Löwen H and Wagner H 1993 *Europhys. Lett.* **22** 245

[37] Whitlock P A, Ceperley D M, Chester G V and Kalos M H 1979 *Phys. Rev.* B **19** 5598

[38] Kalos M H, Levesque D and Verlet L 1974 *Phys. Rev.* A **9** 2178

[39] Likos C N and Aschcroft N W 1992 *Phys. Rev. Lett.* **69** 316; 1992 **69** 3141E; 1993 *J. Chem. Phys.* **99** 9090

[40] Krotscheck E private communication.

[41] Stringari S 1992 *Phys. Rev.* B **46** 2974; Dalfovo F and Stringari S 1992 *Phys. Rev.* B **46** 13991; 1992 *J. Low Temp. Phys.* **89** 325
[42] Puff R D 1965 *Phys. Rev.* **137** A 406
[43] Holas A 1987 in *Strongly Coupled Plasma Physics* edited by Rogers F J and Dewitt H E (New York: Plenum)

Tables and table captions

Table 1. Freezing parameters for the ground-state Bose and Fermi hard-sphere systems: Liquid and solid (*fcc*-crystal) coexistence densities, ρ_l and ρ_s, density change $\Delta\rho$, Gaussian width parameter α, and Lindemann ratio L.

	$\rho_l\sigma^3$	$\rho_s\sigma^3$	$\Delta\rho\sigma^3$	$\alpha\sigma^2$	L
Bose Hard Spheres:					
Theory (PPA-HNC)	0.351	0.365	0.014	14.38	0.206
Theory (PPA-HNC+)	0.359	0.371	0.012	13.39	0.214
Simulation	0.23±.02	0.25±.02	0.02	6.25	0.27
Fermi Hard Spheres:					
Theory (PPA-HNC+)	0.313	0.326	0.013	10.24	0.235

Table 2. Liquid-state numerical data corresponding to Figures 6 and 7: Predicted ground-state energy densities over a range of number densities ρ for the Bose hard-sphere liquid (E^B/V) in the HNC and HNC+ approximations and for the Fermi hard-sphere liquid (E^F/V) in the HNC+ approximation.

$\rho\sigma^3$	E^B/V (HNC)	E^B/V (HNC+)	E^F/V (HNC+)
0.02	0.0043	0.0044	0.0068
0.04	0.0205	0.0204	0.0290
0.06	0.0539	0.0524	0.0702
0.08	0.1099	0.1052	0.1345
0.10	0.1945	0.1842	0.2266
0.12	0.3141	0.2954	0.3521
0.14	0.4760	0.4452	0.5174
0.16	0.6883	0.6411	0.7295
0.18	0.9601	0.8909	0.9964
0.20	1.3018	1.2036	1.3271
0.22	1.7252	1.5889	1.7313
0.24	2.2434	2.0574	2.2198
0.26	2.8713	2.6210	2.8045
0.28	3.6257	3.2925	3.4981
0.30	4.5252	4.0857	4.3147
0.32	5.5906	5.0159	5.2693
0.34	6.8451	6.0996	6.3781
0.36	8.3141	7.3546	7.6586
0.38	10.0257	8.8000	9.1294

Table 3. Solid-state numerical data corresponding to Figures 6 and 7: Predicted ground-state energy densities over a range of number densities ρ for the hard-sphere solid (E/V) – independent of statistics – in the HNC and HNC+ approximations.

$\rho\sigma^3$	E/V (HNC)	E/V (HNC+)
0.26	3.3346	3.0779
0.28	4.0648	3.7279
0.30	4.8955	4.4608
0.32	5.8279	5.2754
0.34	6.9521	6.2449
0.36	8.2973	7.3914
0.38	9.8544	8.7044
0.40	11.6209	10.1785
0.42	13.5754	11.8113
0.44	15.7220	13.5863

Figure captions

Figure 1. Static structure factor $S(k)$ vs. wave vector magnitude k for Bose hard-sphere liquids of three different densities, generated by the PPA with the HNC+ approximation (see text).

Figure 2. Quantum direct correlation function $v(k)$, corresponding to $S(k)$ in Figure 1, computed from the Feynman approximation [equation (26)]. Vertical bars indicate positions of *fcc* reciprocal lattice vectors at average solid density $\rho_s\sigma^3 = 0.4$, for which the Gaussian width parameter $\alpha\sigma^2 = 15.8$. Bar heights, arbitrarily normalized to 50, are proportional to the product of degeneracy and the Gaussian factor in (34), and thus represent relative contributions to the weighted density $\hat{\rho}$.

Figure 3. First three terms in the Wu-Feenberg cluster expansion, representing Fermi-statistics corrections to the Bose hard-sphere liquid energy per particle (units of $\hbar^2/m\sigma^2$).

Figure 4. Hard-sphere solid energy density (units of $\hbar^2/m\sigma^5$) vs. Gaussian width parameter (solid line) for average solid density $\rho_s\sigma^3 = 0.37$. Shown separately are ideal-gas energy (short-dashed line) and correlation energy (long-dashed line).

Figure 5. Weighted density vs. average solid density at the energy minimum for the hard-sphere *fcc* crystal.

Figure 6. Bose hard-sphere liquid and solid energy densities vs. density, generated for the liquid by the PPA and for the solid by density-functional theory (DFT). Dashed lines correspond to the simple HNC approximation, solid lines to the enhanced HNC+ approximation (see text). Circles and squares denote variational Monte Carlo (VMC) data [22] for the liquid and solid, respectively.

Figure 7. Fermi hard-sphere liquid and solid energy densities vs. density, generated for the liquid by the PPA, with the HNC+ approximation and Wu-Feenberg corrections (see Figure 3 and text), and for the solid by DF theory. Dashed line shows the Bose liquid energy density from Figure 6, illustrating the approximate magnitude of statistics corrections in the liquid. Circles and squares denote VMC data [29] for the liquid and solid, respectively.

Fig. 1 (Denton et al)

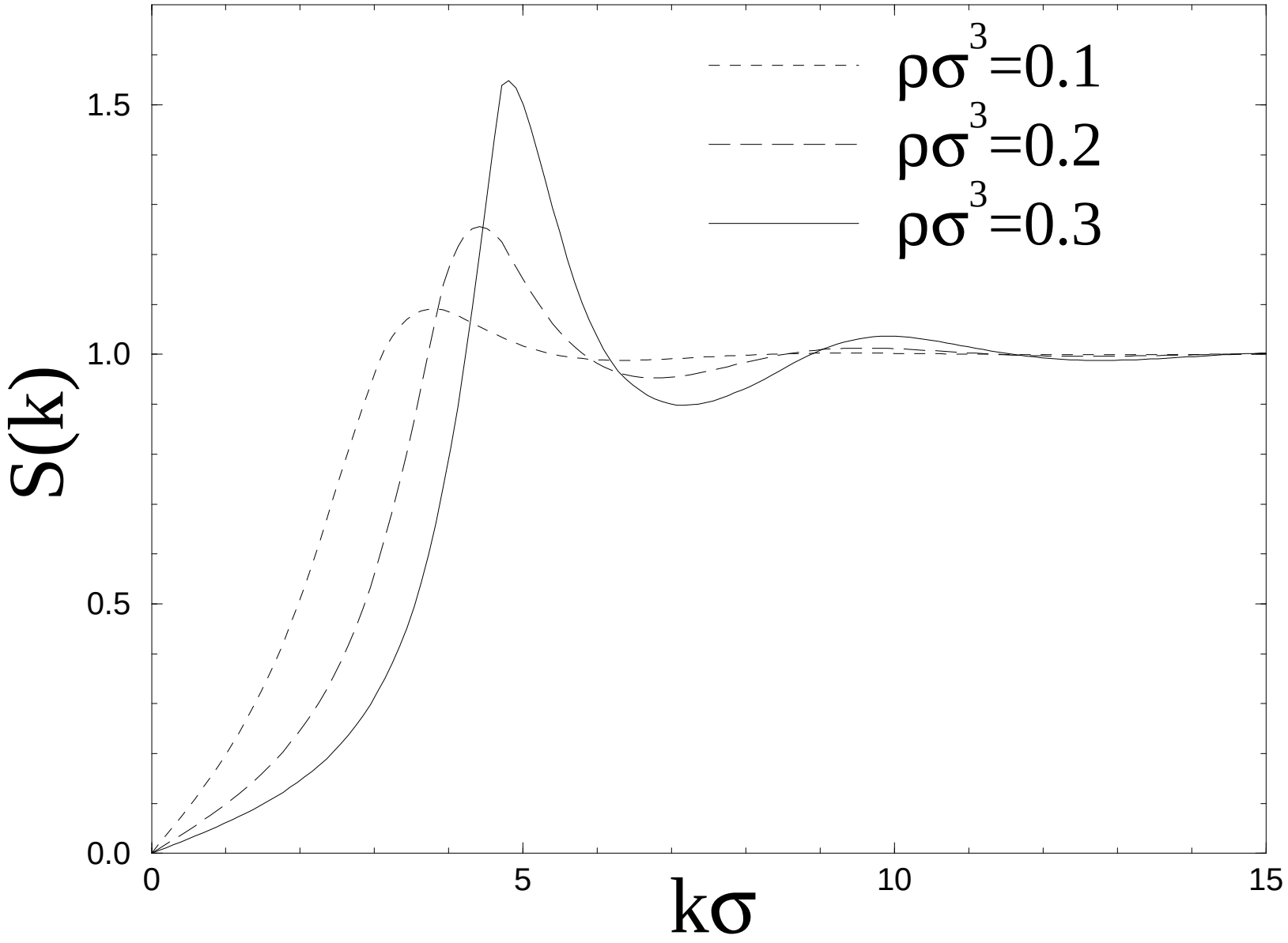

Fig. 2 (Denton et al)

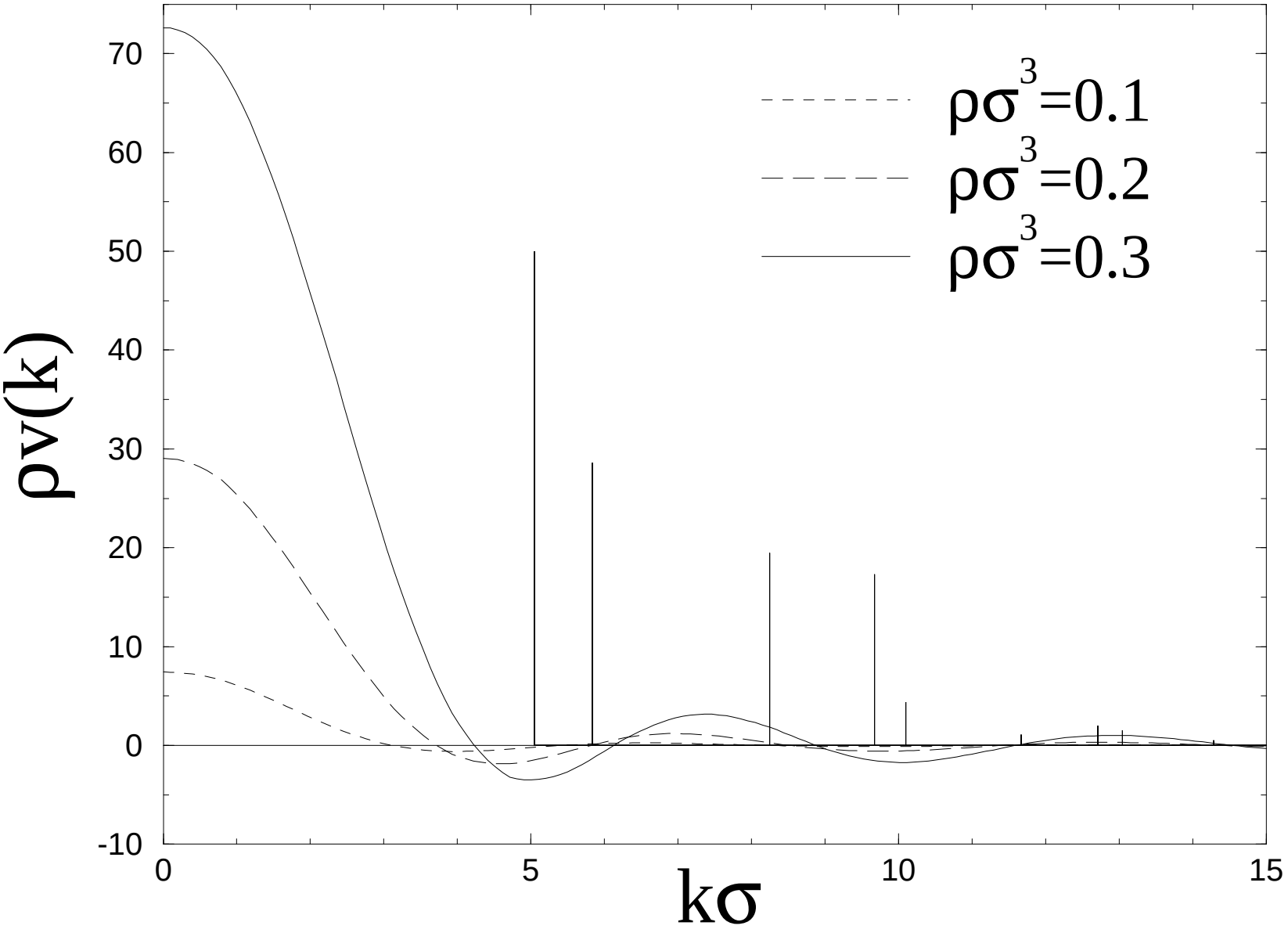

Fig. 3 (Denton et al)

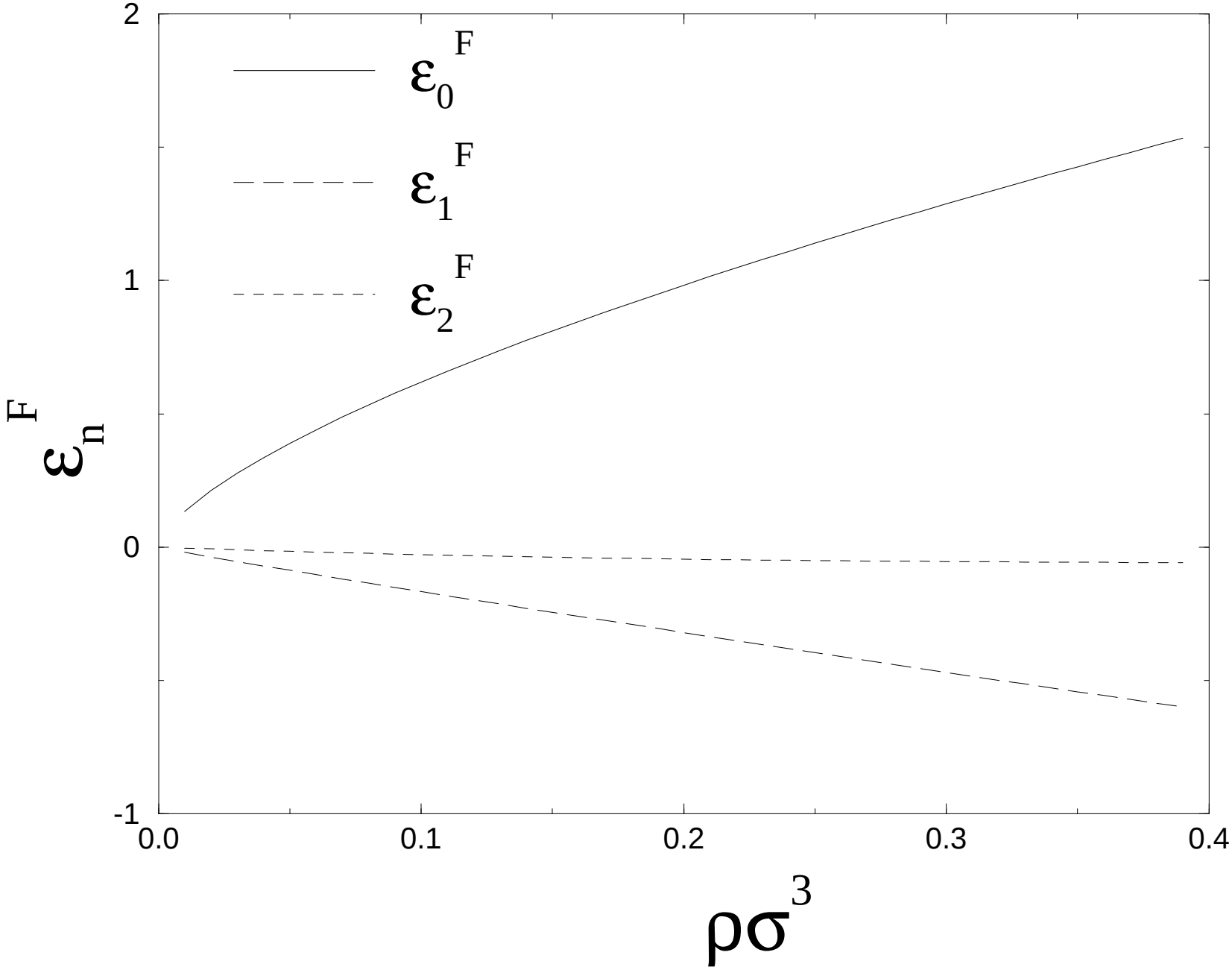

Fig. 4 (Denton et al)

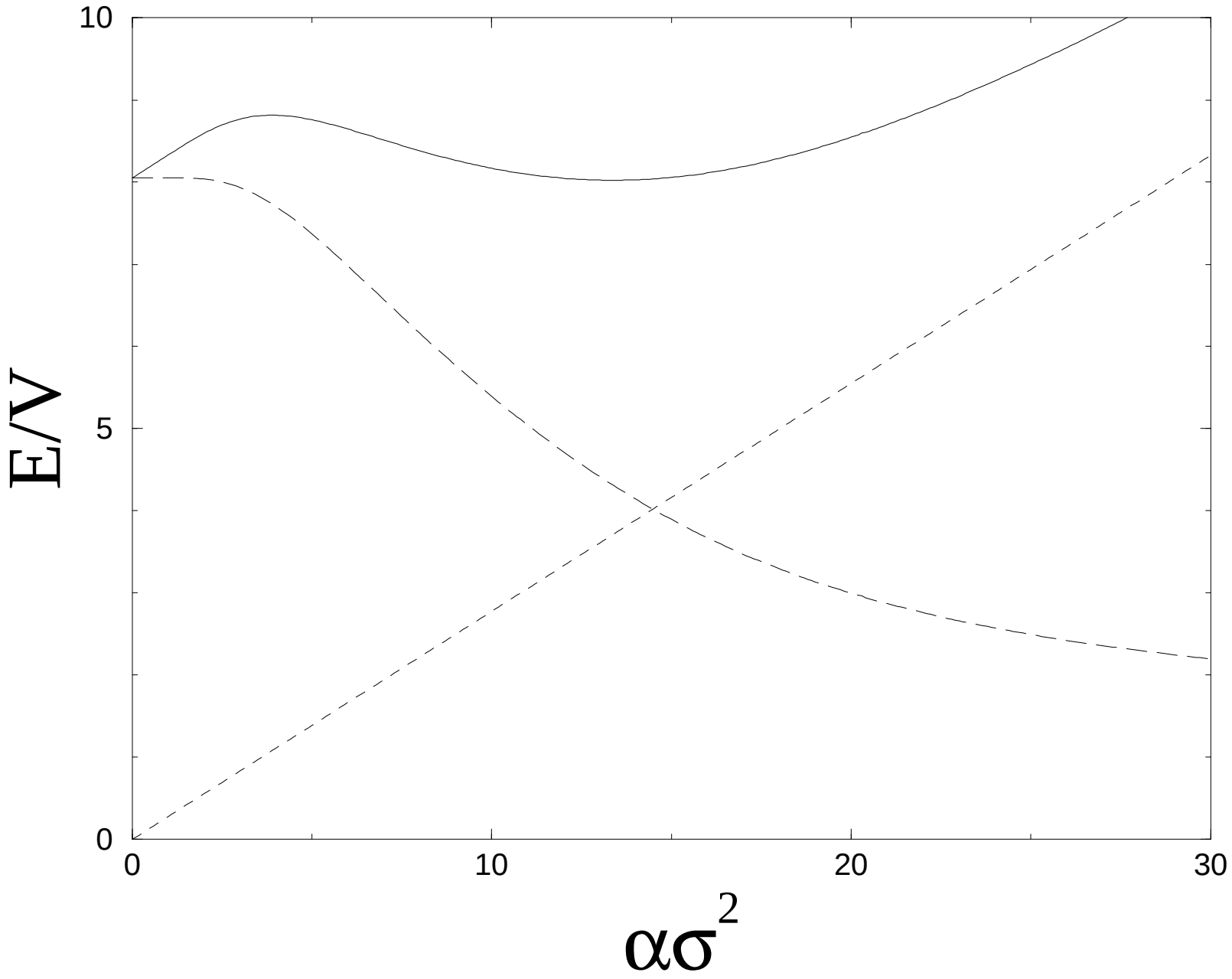

Fig. 5 (Denton et al)

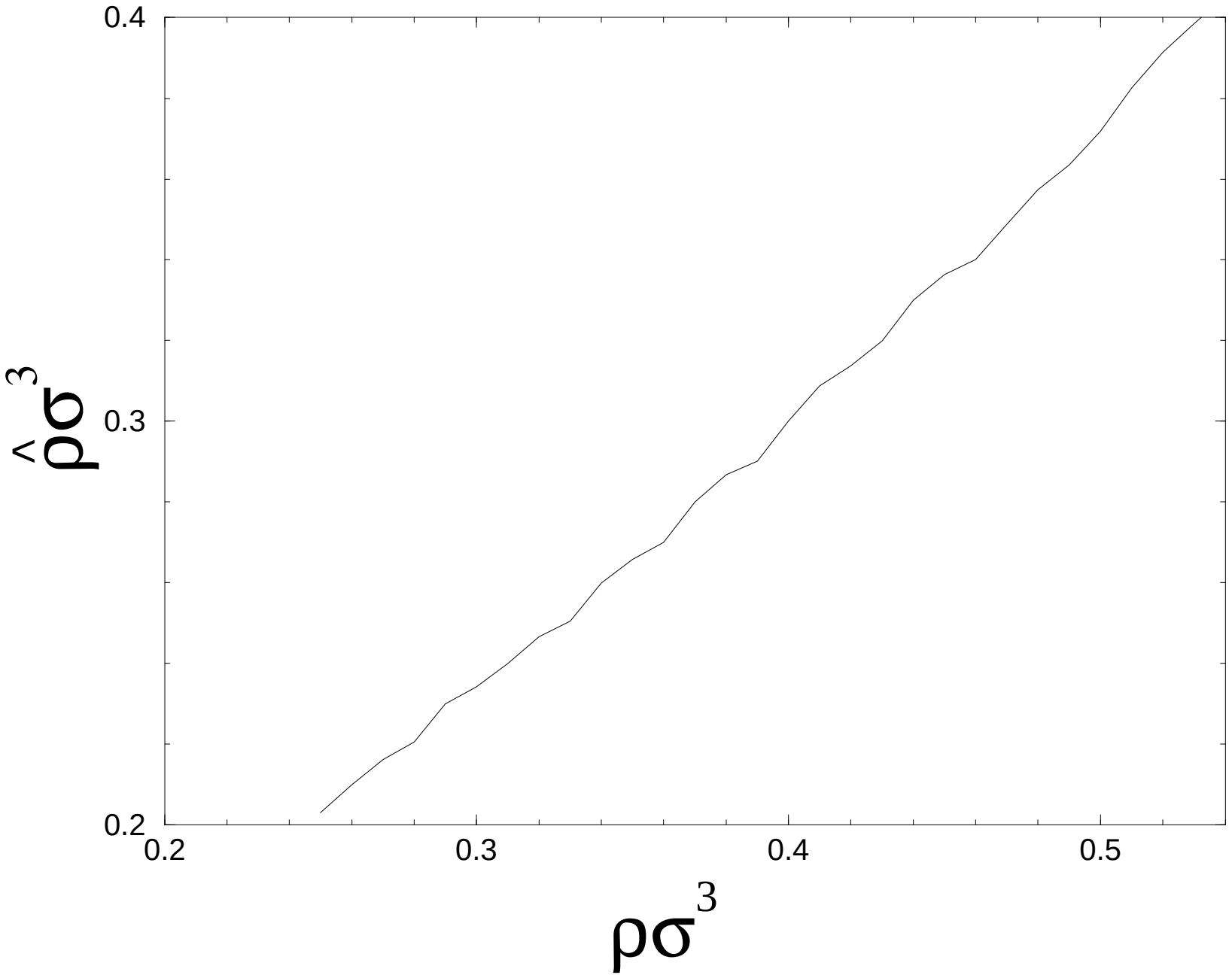

Fig. 6 (Denton et al)

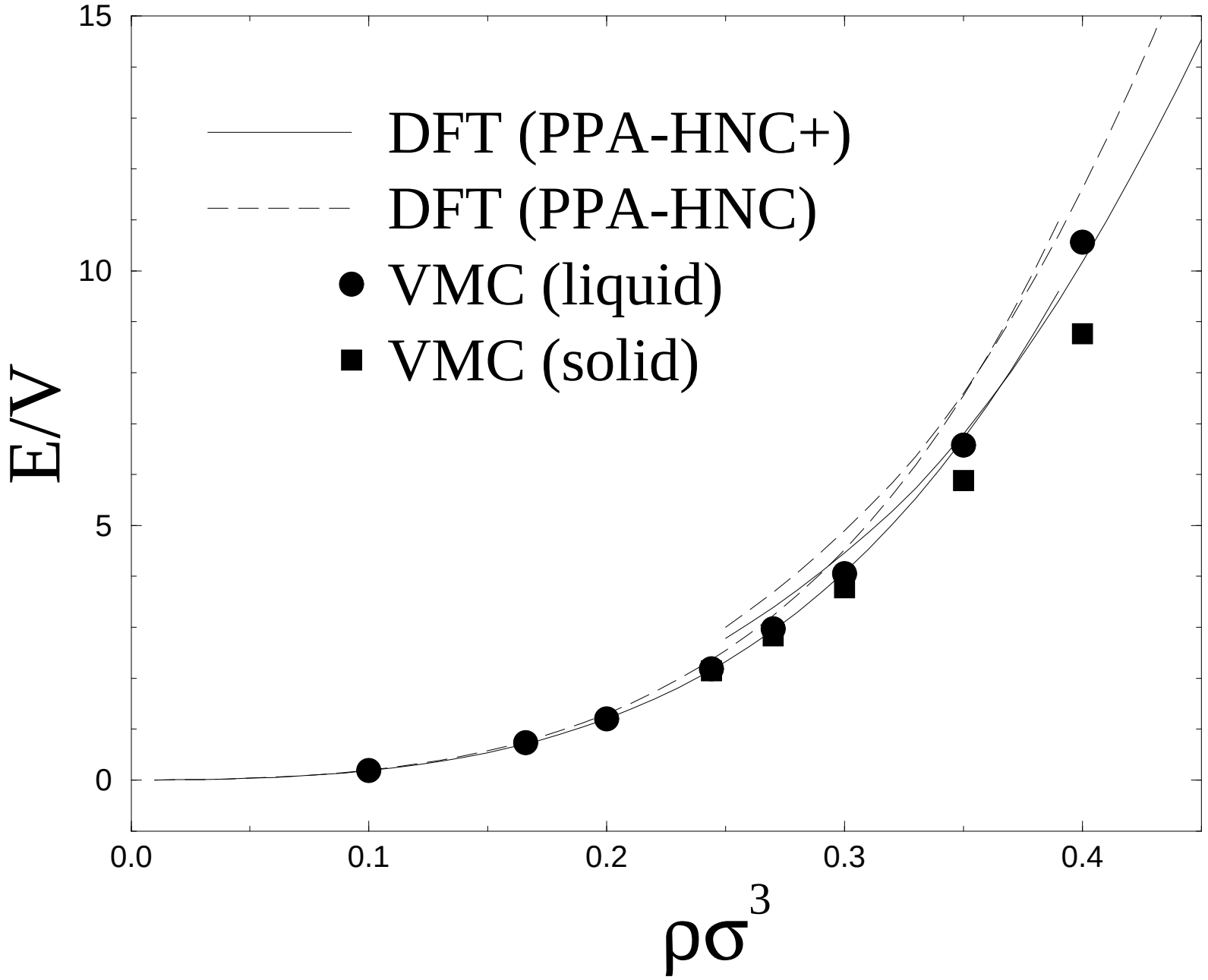

Fig. 7 (Denton et al)